Molecular curvature, specific intermolecular interactions and the twist bend nematic phase: the synthesis and characterisation of the 1-(4-cyanobiphenyl-4′-yl)-6-(4-alkylanilinebenzylidene-4′-oxy)hexanes (CB6O.*m*)

Rebecca Walker[a], Damian Pociecha[b], Grant J Strachan[a], John MD Storey[a], Ewa Gorecka[b] and Corrie T Imrie[a]

Department of Chemistry, School of Natural and Computing Sciences, University of Aberdeen, AB24 3UE Scotland, United Kingdom; University of Warsaw, Faculty of Chemistry, ul. Zwirki i Wigury 101, 02-089 ˙ Warsaw, Poland

E-mail: c.t.imrie@abdn.ac.uk

Abstract

The syntheses and characterisation of the first ten homologues of the 1-(4-cyanobiphenyl-4′-yl)-6-(4-alkylanilinebenzylidene-4′-oxy)hexanes (CB6O.*m*) are reported. All ten members of the series exhibit an enantiotropic nematic, N, phase, and a monotropic twist-bend nematic, $N_{TB,}$ phase. Only CB6O.10 shows a smectic phase. The assignment of both nematic phases was confirmed using X-ray diffraction. For short chain lengths (*m*=1-6) the local packing in both nematic phases is an intercalated arrangement, for intermediate chain lengths a frustrated local structure is seen and for the longest chain length, a bilayer arrangement is observed. This change in the local structure on increasing *m* has no apparent effect on the stability of either nematic phase, and $T_{N_{TB}N}$ and T_{NI} show a regular dependence on *m*. Specifically, $T_{N_{TB}N}$ and T_{NI} decrease on increasing *m* and superimposed upon this is a weak odd-even effect in which the odd members show the higher values. T_{NI} decreases more rapidly than $T_{N_{TB}N}$ on increasing *m* such that the ratio $T_{N_{TB}N}$/ T_{NI} increases. The lower temperature liquid crystal phase shown by 1-(4-cyanobiphenyl-4′-yloxy)-5-(4-butylanilinebenzylidene-4′-oxy)pentane (CBO5O.4) is reassigned as a twist-bend nematic phase. The transitional properties of the CB6O.*m*, CB6O.O*m* and CBO5O.*m* series are compared.

Keywords: liquid crystals, helical structures, twist-bend nematic phase, liquid crystal dimers, X-ray diffraction, smectic phases.

Introduction

The twist-bend nematic phase, N_{TB}, is presently the focus of intense research activity for a number of reasons but perhaps primarily because it is the first example of spontaneous chiral symmetry breaking in a fluid with no spatial ordering [1-3].The N_{TB} phase was first predicted over 35 years ago by Meyer [4] and subsequently independently by Dozov [5] prior to its experimental discovery a decade later [1]. At the heart of Dozov's seminal work is the assertion that bent molecules have a natural tendency to pack into bent structures. Pure uniform bend in space, however, is not allowed, and must be accompanied by other local deformations of the director, namely splay or twist [5]. The splay-bend nematic phase is achiral whereas in the twist-bend nematic, N_{TB}, phase the director forms a heliconical structure in which it is tilted with respect to the helical axis. Left- and right-handed helices are degenerate and thus expected to form in equal amounts. The pitch length in the N_{TB} phase is strikingly small, corresponding typically to just 3-4 molecular lengths [2, 3]. In the overwhelming majority of cases, the N_{TB} phase is preceded by a conventional nematic phase, N, although direct N_{TB}-isotopic phases have been observed [6-8]. The N phase preceding a N_{TB} phase is of interest in its own right, possessing an anomalously low bend elastic constant and has considerable application potential [9-11].

The essential molecular requirement for the observation of the N_{TB} phase is widely thought to be a bent shape and this is in accord not only with Dozov's prediction[5] but also with Maier-Saupe theory for V-shaped molecules which predicts the N_{TB}-N transition temperature to be particularly sensitive to the bend angle and the N_{TB} phase will form for just a narrow range of molecular curvatures [12]. By far the most common molecular architecture used to obtain the N_{TB} phase is that of liquid crystal dimers in which two mesogenic units are linked through a flexible methylene spacer [13, 14]. If the two mesogenic groups in a dimer are connected by an odd number of atoms then the molecule is bent, and the material has the potential to exhibit the N_{TB} phase. A relatively large and growing number of odd-membered dimers have now been reported to show the N_{TB} phase (see, for examples, references [15-30]). Other types of structures have been shown to support the N_{TB} phase such as rigid bent core liquid crystals [31, 32], higher oligomers such as trimers, tetramers and hexamers [33-35] and hydrogen-bonded sytems [36-38].

Using symmetry arguments, Dozov not only predicted the N_{TB} phase but also the existence of helical smectic phases consisting of achiral molecules [5]. This has been a difficult prediction to verify because the great majority of N_{TB} phases either vitrify or crystallise on cooling, and only rarely have smectic-N_{TB} or B-N_{TB} phase transitions been observed [7, 39-41]. Recently, however, we have shown that members of the CB6OIBeO*n* series,

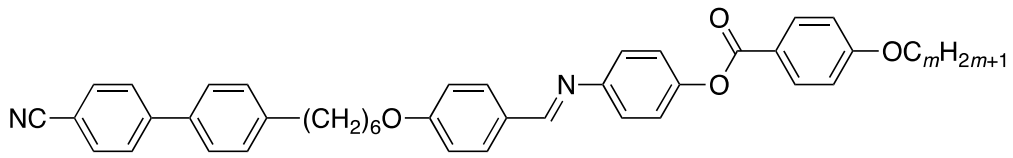

do indeed form heliconical smectic phases, specifically the SmC_{TB} phase in which the director forms a helix and is tilted with respect to the helical axis [42]. A helical smectic phase formed by achiral molecules has been suggested also for a rigid bent core liquid crystal [43].

In order to better understand how these bent dimers pack into smectic phases and their properties, we reported the transitional properties of the CB6O.O*m* series,

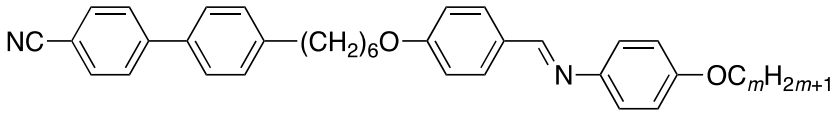

and a monotropic intercalated, anticlinic smectic C phase was seen for *m*=3,4 and 5 [44, 45]. The absence of smectic behaviour for other members of the series was attributed to both the inherent difficulty associated with packing bent molecules into layered arrangements, and for these intercalated structures the necessity to accommodate the terminal chains within the space between the mesogenic units which is determined by the length of the flexible spacer [46]. Clearly we are at a very early stage in developing our understanding of the smectic behaviour seen for these bent molecules and how the anomalously low bend elastic constants affect the structures of these new phases. The first stage of this work must be the design and synthesis of a wider range of materials that exhibit these new heliconical smectic phases. Thus, in order to better understand how changing molecular structure promotes smectic behaviour in odd-membered dimers, here we report a set of

materials structurally similar to the previously reported CB6O.O*m* series, the 1-(4-cyanobiphenyl-4′-yl)-6-(4-alkylanilinebenzylidene-4′- oxy)hexanes,

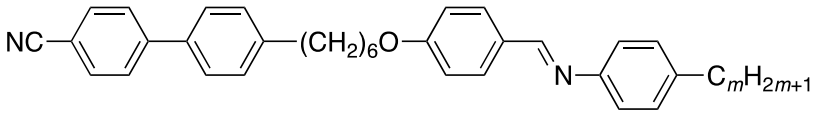

and by analogy refer to them using the acronym CB6O.*m* in which *m* denotes the number of carbon atoms in the terminal alkyl chain and this has been varied from 1 to 10. Although the change from an alkyloxy to an alkyl chain may appear a very subtle one, in conventional low molar mass systems it can give rise to significant differences in behaviour. This particular structure has been chosen because the hexyloxy spacer imparts the molecular curvature required for the observation of twist-bend phases [42, 47], and the cyanobiphenyl and Schiff base units show a favourable specific interaction that drives the formation of smectic phases in dimers and higher oligomers [48-50]. This series will allow us to further address the question of the importance of intercalation in both the formation of the N_{TB} [29, 51, 52] and smectic phases[46]. We compare the properties of the CB6O.*m* series to those of both the corresponding dimers containing an alkyloxy chain, the CB6O.O*m* series,[44] and the analogous ether-linked materials, the CBO5O.*m* series [48, 49]:

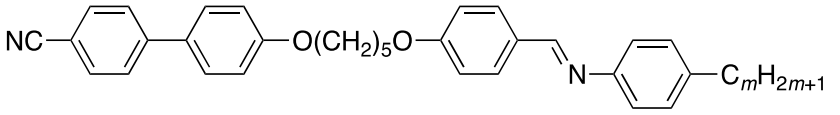

.

Experimental

Synthesis

The synthetic route used to obtain the CB6O.*m* series is shown in the Scheme. The synthesis of 4-{4-[6-(4-formylphenoxy)hexyl]phenyl}benzonitrile (**1**) has been described elsewhere [42]. A detailed description of the reaction of **1** with the appropriate 4'-alkylaniline to give a CB6O.*m* dimer is provided in the Supplementary Information along with structural characterisation and purity data for all final products. The synthesis and characterisation of CBO5O.4 is also fully described in the Supplementary Information.

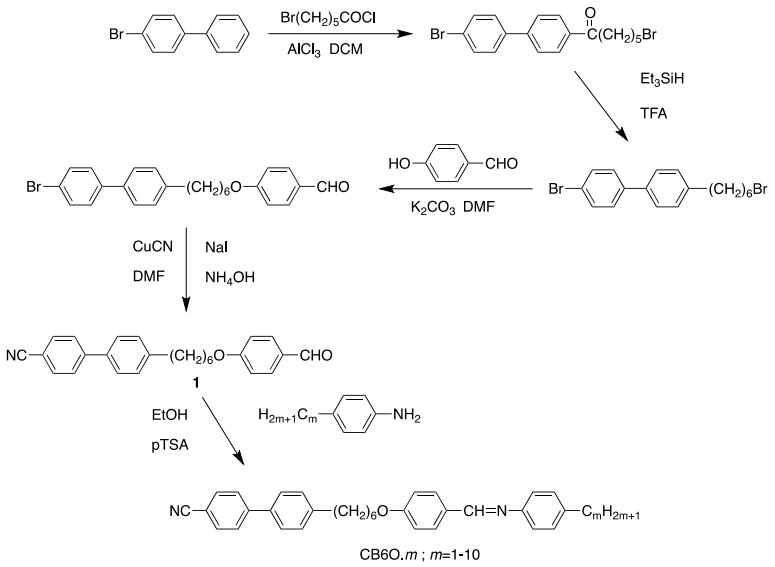

Scheme Synthesis of the CB6O.*m* series.

Thermal Characterisation

The phase behaviour of the dimers was studied by differential scanning calorimetry using a Mettler-Toledo DSC820 fitted with an intracooler and calibrated using indium and zinc as standards. Heating and cooling rates were 10 ˚C min^{-1} and all samples were measured under a nitrogen atmosphere. Transition temperatures and associated enthalpy changes were extracted from the second heating trace unless otherwise noted. For each sample, two aliquots were measured and the data listed are the average of the two sets of data. The DSC instrument used has a temperature accuracy of ±0.2 K, temperature precision of ±0.02 K and calorimetric resolution of 0.04 μW. We note that the experimental uncertainty associated with the reported entropy values are not dependent on the instrument specifications, but rather on the subjective peak analyses. These errors depend strongly on the peak shape and area, and as such will vary in magnitude between strongly first order transitions, for example a crystal-isotropic melt, and those which are weakly first order or tend towards being second order in nature, such as the twist-bend nematic-nematic phase transition. Small values of the scaled entropy reported of the order of 10^{-2} indicate that an enthalpy change is discernible, however these are subject to a large degree of error depending on how the shape of the endotherm is interpreted, *ie*. the placement of integration limits. Alternatively, one could regard such an endotherm as a pseudo-second order step-change in the heat flow baseline and report the thermodynamic parameters as ~0. Phase characterisation was performed using polarised light

microscopy using an Imager A2m polarizing microscope equipped with a Linkam heating stage.

X-ray diffraction

Wide angle diffractograms (WAXS) were obtained with a Bruker D8 GADDS system (CuKα line, Goebel mirror, point beam collimator, Vantec2000 area detector). Samples were prepared as droplets on a heated surface.

Molecular Modelling

In order to establish the geometric parameters of the dimers quantum mechanical density functional theory was used. Geometric optimisation on both the molecular fragments and the dimers with the spacer in the all-*trans* conformation was performed using Gaussian G09W at the B3LYP/6-31G(d) level of theory. The all-*trans* conformers were exclusively selected even though calculations for similar sets of dimers of identical spacer length consistently show that in the ground state the spacers contain a gauche defect about the O-C-C-C dihedral (≈±62°) [29, 47, 53]. The difference in energy between the calculated ground state and all-*trans* conformations is small, typically around 1 kJ mol^{-1}, and is likely to be substantially different in an ordered liquid crystal phase which will preferentially select more linear conformations [54]. Thus, we consider the all-*trans* conformation to be a better representation of the average molecular shape in discussing the transitional properties of these dimers. Visualisation of space-filling models of the output post-optimisation was performed using QuteMol [55].

Results and Discussion

The transition temperatures and associated entropy changes of the CB6O.*m* series are listed in Table 1. All ten members of this series exhibit an enantiotropic conventional nematic phase, N, and a monotropic twist-bend nematic phase, N_{TB}. On heating, the DSC trace for each member of the series contained a strong lower temperature endotherm associated with the crystal-nematic transition and a weaker higher temperature nematic-isotropic endotherm. On cooling the homologues with *m*=1-9, an additional very weak exotherm was observed associated with the N_{TB}-N

transition. The N phase was assigned on the basis of the observation of a characteristic schlieren texture containing both two and four brush point singularities and which flashed when subjected to mechanical stress when sandwiched between untreated glass slides and viewed through the polarised optical microscope. The values of $\Delta S_{NI}/R$ obtained are wholly consistent with those expected for odd-membered dimers [56, 57]. On cooling, the nematic schlieren texture changed to give rope-like and focal-conic textures characteristic of the N_{TB} phase, and the transition was accompanied by the cessation of the optical flickering associated with director fluctuations in the N phase. The entropy changes associated with the N_{TB}-N transition are small and consistent with the relatively long temperature range of the preceding N phase [53]. Representative DSC traces and optical textures observed for samples sandwiched between untreated glass slides for CB6O.4 are shown in Figure 1. For samples contained in 1.6 μm cells with planar anchoring, a uniform texture was obtained for the conventional nematic phase and on cooling into the N_{TB} phase a striped texture developed, see Figure 2, and again the transition was associated with the cessation of optical flickering.

Table 1. Transition temperatures and associated entropy changes for the CB6O.*m* series.

m	T_{Cr-}/ °C	$T_{SmN_{TB}}$/ °C	$T_{N_{TB}N}$ / °C	T_{NI}/ °C	ΔH_{Cr-} / kJmol^{-1}	$\Delta H_{N_{TB}N}$/ kJmol^{-1}	ΔH_{NI} / kJmol^{-1}	ΔS_{Cr-}/ R	$\Delta S_{N_{TB}N}$/ R	ΔS_{NI}/ R
1	112		88	129	20.26	0.17	0.78	6.33	0.06	0.23
2	117		80	122	25.88	0.06*	0.57	7.98	0.02*	0.17
3	120		86	126	34.19	0.26	0.80	10.46	0.09	0.24
4	103		75	115	28.48	0.33	1.04	9.11	0.11	0.20
5	89		79	117	25.49	0.42	0.94	8.47	0.14	0.29
6	80		69	107	38.14	0.15	0.58	12.99	0.05	0.18
7	89		73	109	36.60	0.20	0.91	12.16	0.07	0.29
8	90		64	96	32.95	0.26	0.58	10.91	0.09	0.19
9	77		71	103	34.14	0.13	0.84	11.73	0.05	0.27
10	89	67	73	101	53.32	0.75†	0.74	17.71	0.26†	0.24

*Exotherm partially overlapped with crystallisation peak. †Entropy change represents the combined smectic-twist-bend nematic (Sm-N_{TB}) and N_{TB}-N phase transitions.

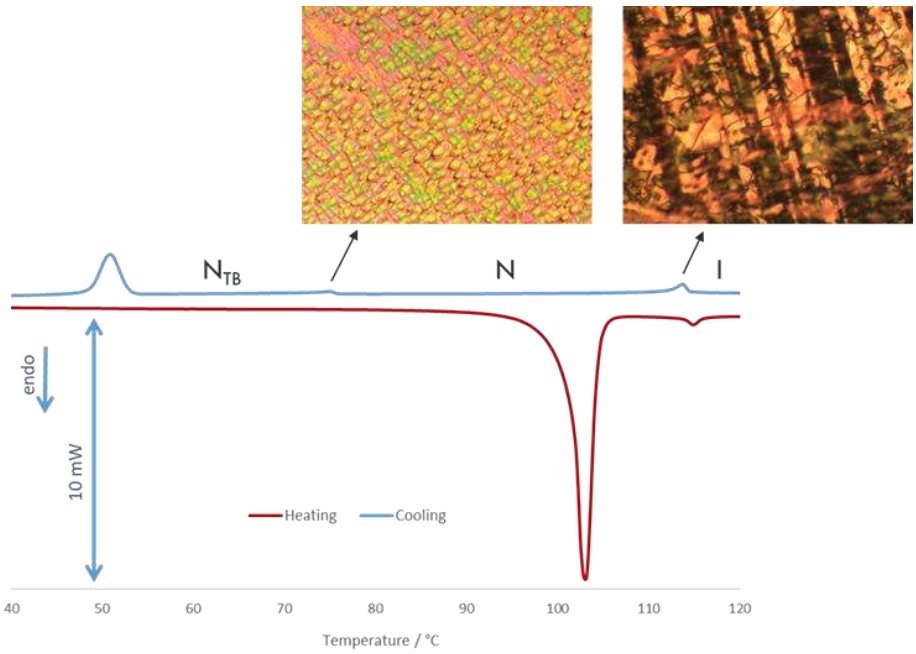

Figure 1. The DSC traces obtained on heating and cooling for CB6O.4. Also shown are the optical textures observed for the N_{TB} (left) and N (right) phases for samples sandwiched between untreated glass slides.

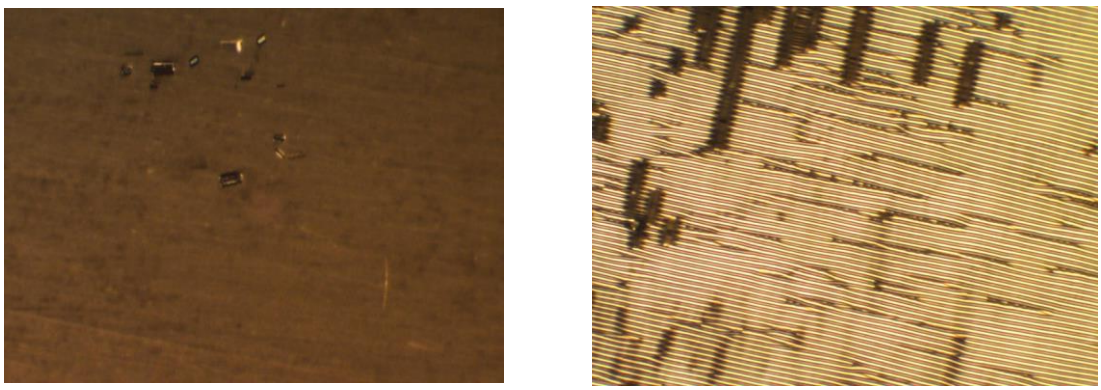

(a) (b)

Figure 2. (a) The uniform texture of the nematic phase and (b) the striped texture in the N_{TB} phase observed for CB6O.4 in a 1.6 μm cell with planar anchoring.

On cooling the N_{TB} phase for CB6O.10 a smectic phase develops which, like the preceding N_{TB} phase, exhibits a striped texture in a cell treated for planar anchoring whereas in a cell with homeotropic anchoring a uniformly black texture was seen. Similar textures were observed for the SmC_{TB} phase [42]. Conventional X-ray diffraction suggests a smectic phase with liquid-like ordering within the layers, see Figure 3. However, resonant soft X-ray scattering measurements have revealed a complex phase structure and a detailed discussion of this phase will be presented elsewhere [58].

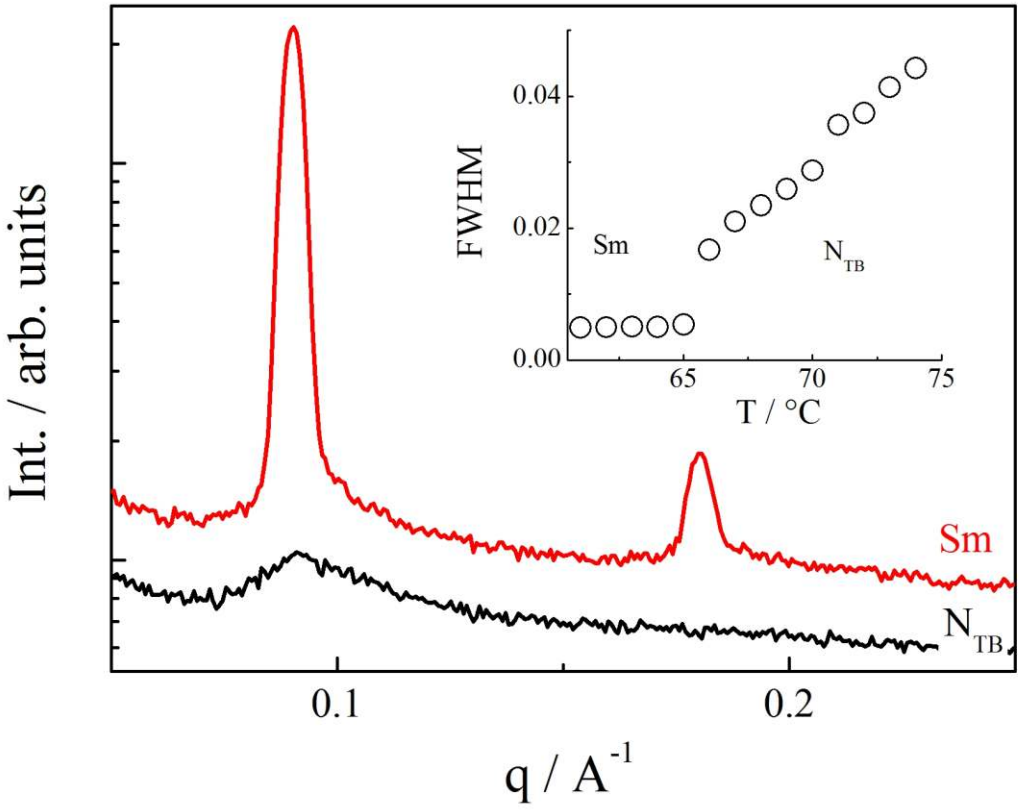

Figure 3. The intensity profiles of the X-ray patterns for the smectic and N_{TB} phases shown by CB6O.10. The inset shows the FWHM of the small angle diffraction peak in both phases.

X-ray diffraction was used to confirm the assignments of the N and N_{TB} phases. The X-ray patterns obtained for both nematic phases are essentially identical consisting of broad signals indicative of a liquid-like arrangement of the molecules (Figures 4(a) and (b)). The local periodicities, *d,* in the nematic phases deduced from

the peak positions in the small angle region of the X-ray patterns are listed in Table 2. The ratios of these periodicities in the nematic phases for *m*=1-6 to their molecular lengths, *l,* lie in the range 0.5-0.6 suggesting a locally intercalated arrangement of the molecules. This is often observed for the N_{TB} phase and thought to be associated with the packing of bent molecules. For *m*=7 and 8, three broad signals are observed in the low angle region of the X-ray patterns of both nematic phases at positions corresponding to values of *d/l* of approximately 0.6, 1.0 and 1.8. This suggests a frustrated local structure in the nematic phases involving intercalated, monolayer and interdigitated packing arrangements. For the longest terminal chain length, *m*=10, the X-ray pattern of the conventional nematic phase contains two broad signals in the low angle region at positions corresponding to the molecular length and twice the molecular length and in the N_{TB} phase the latter reflection is the dominant one, see Figure 5. These data appear to indicate that the local structure in both nematic phases changes from being intercalated for short terminal chains, shows a degree of frustration for intermediate chain lengths, to adopt a bilayer structure for the longest chain length, *m*=10 (Figure 3). To our knowledge this is the first time that this progression of local structure has been observed within a series exhibiting the N_{TB} phase and surprisingly appears to have no appreciable effect on the stability of either N phase. Specifically, a regular dependence of both T_{NI} and $T_{N_{TB}N}$ is seen on increasing *m*, see Figure 6, suggesting that the importance of the intercalation of the molecules in stabilising the N_{TB} phase may have been overstated and this will be discussed later.

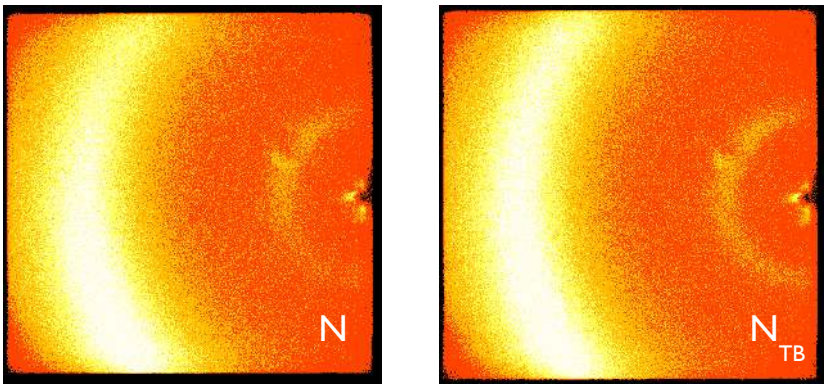

(a) (b)

Figure 4. X-ray diffraction patterns of CB6O.4 in (a) the N phase and (b) the N_{TB} phase.

m	**Phase**	***d* / Å**	***l* / Å**	***d*/*l***
1	N	13.7	25.9	0.53
	N_{TB}	13.4		0.52
4	N	15.6	28.1	0.56
	N_{TB}	15.6		0.56
6	N	16.4	29.5	0.56
	N_{TB}	16.7		0.57
7	N_{TB}	53.8, 28.7, 18.1	30.1	1.79, 0.95, 0.58
8	N_{TB}	58.4, 34.2, 18.4	31.2	1.87, 1.10, 0.59
10	N	66.4, 32.6	32.8	2.02, 0.99
	N_{TB}	66.4		2.02

Table 2. The periodicities in the N and N_{TB} phases, *d*, deduced from the position of the small angle peak in the X-ray patterns, the estimated *all*-trans molecular lengths, *l*, and the *d*/*l* ratios for members of the CB6O.*m* series.

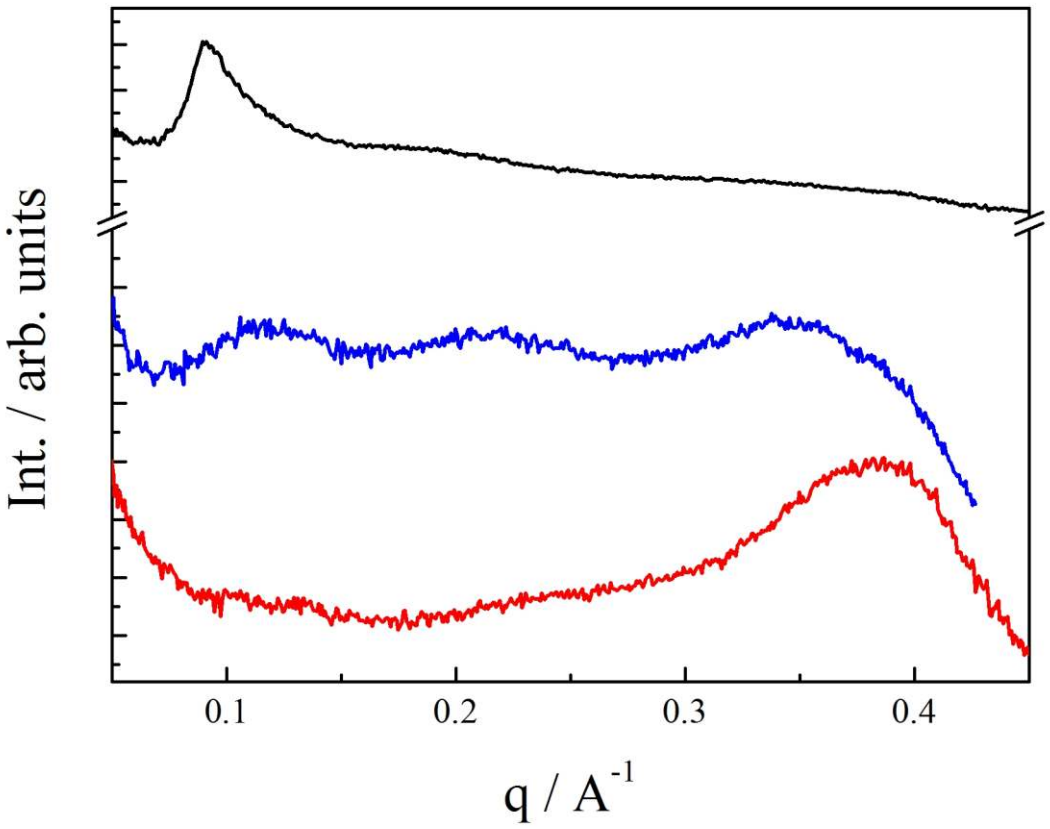

Figure 5. The intensity profiles of the X-ray patterns of the N_{TB} phases shown by CB6O.4 (bottom), CB6O.7 (middle) and CB6O.10 (top). The curves have been shifted along the vertical axis for clarity.

The dependence of the transition temperatures on the terminal alkyl chain length, *m*, is shown in Figure 6. The nematic-isotropic transition temperature, T_{NI}, tends to decrease on increasing *m* and superimposed on this trend is a weak odd-even effect in which the odd members show the higher values, and similar behaviour was seen for the CB6O.O*m* series [44]. Increasing the length of a terminal chain has two effects on T_{NI}: first, the shape anisotropy is enhanced, increasing T_{NI} and the effect on shape is greater for odd rather than even members of a methylene-linked chain giving the observed alternation in T_{NI}; secondly, increasing the terminal chain length dilutes the interactions between the mesogenic units which serves simply to decrease T_{NI}. The overall effect of increasing the length of a terminal chain, therefore, depends on the interaction strength parameter between the mesogenic units [59] and for these dimers it is apparent that the dilution effect dominates reducing T_{NI} but with a

weak alternation. The entropy changes associated with the nematic-isotropic transition scaled by the gas constant, $\Delta S_{NI}/R$, are listed in Table 1 and these are small and rather similar. Although there is evidence of a weak odd-even effect in these values, this approaches the limits of experimental error, and the values suggest that the increase in conformational entropy arising from the increased chain length is small compared to the overall entropy change.

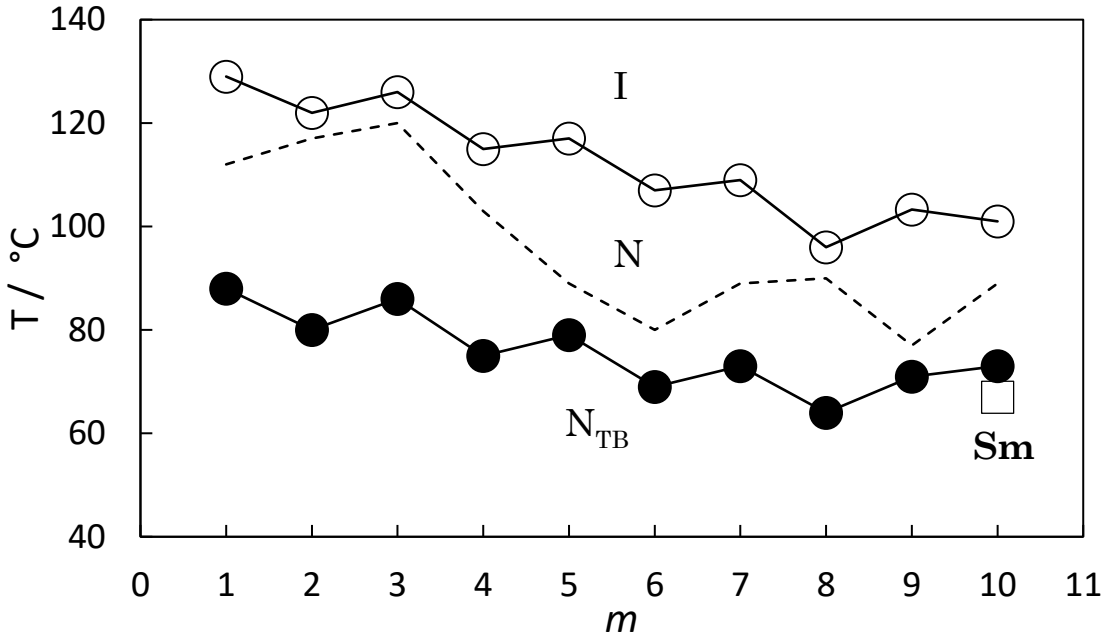

Figure 6. The dependence of the transition temperatures on the number of carbon atoms in the terminal alkyl chain, *m*, for the CB6O.*m* series. Open circles represent nematic-isotropic transition temperatures and filled circles twist-bend nematic-nematic transition temperatures. The broken line connects the melting points. The open square denotes a smectic-twist-bend nematic transition temperature.

The dependence of the N_{TB}-N transition temperature, $T_{N_{TB}N}$, on *m* is qualitatively the same as that seen for T_{NI} and similar behaviour was observed for the CB6O.O*m* series [44]. Thus, $T_{N_{TB}N}$ decreases, albeit to a lesser extent than T_{NI}, on increasing *m* and superimposed upon this decrease is a small odd-even effect in which the odd members have the higher values. The width of the N phase decreases

on increasing *m* such that the $T_{N_{TB}N}$/ T_{NI} ratio increases. The same behaviour was observed for the CB6O.O*m* series and indicates that increased dilution of the interactions between the mesogenic units on increasing *m* has a greater effect on T_{NI} than on the predominantly shape-driven N_{TB}-N transition. It is also noteworthy that the alternations seen for T_{NI} and $T_{N_{TB}N}$ on increasing *m* are in the same sense implying that increasing the linearity of the molecule can simultaneously increase T_{NI} and $T_{N_{TB}N.}$ Such behaviour has now been observed for a number of materials including the CB*n*CB and CB*n*OCB series [47, 53].

We now turn our attention to a comparison between the transitional properties of the CB6O.*m*, CB6O.O*m* [44] and CBO5O.*m* series [49] but before we can do this, we must first revisit the behaviour of the CBO5O.*m* series first reported some 25 years ago [49]. All the members of this series with *m*=1-10 exhibited an enantiotropic nematic phase. In addition, for *m*=1-9 a monotropic smectic phase was observed, and for *m*=10 an enantiotropic SmA and monotropic SmC phase, both having an interdigitated structure, were seen. The authors commented that the dependence of the smectic-nematic transition temperature on *m* was unusual because it decreased essentially without alternation over the first 8 members, rose slightly passing to *m*=9 and then sharply to *m*=10 [49]. The monotropic nature of the smectic phase precluded its characterisation using X-ray diffraction and instead the phase assignment was based entirely on the observation of a focal conic fan texture when viewed through the polarised light microscope. With hindsight, and given the behaviour of the CB6O.*m* series reported here, the monotropic smectic phase assigned for *m*=1-9 may in fact be the N_{TB} phase and to investigate this possibility we synthesised and characterised CBO5O.4. The transitional properties of CBO5O.4 are listed in Table 3 and the transition temperatures are in very good agreement with the literature values [49]. The N phase was assigned on the basis of the observation of a characteristic schlieren texture, see Figure 7. On cooling, a characteristic texture developed strongly suggesting that the lower temperature phase is the N_{TB} phase, see Figure 7, but the monotropic nature of the phase precluded the confirmation of this assignment using X-ray diffraction. Instead we constructed a binary phase diagram for mixtures of CBO5O.4 and the standard twist bend nematogen, CB6OCB[47], see Figure 8. Complete miscibility between the two components was observed over the entire composition range and each mixture exhibited a conventional nematic phase at

higher temperatures and a twist-bend nematic phase on cooling, see Figure 9. Both T_{NI} and $T_{N_{TB}N}$ vary in essentially a linear manner with mixture composition. The value of $T_{N_{TB}N}$ measured for CBO5O.4 fits perfectly on the $N_{TB}N$ line in the phase diagram confirming that the lower temperature phase for CBO5O.4 is indeed the N_{TB} phase.

T_{Cr} / °C	$T_{N_{TB}N}$ / °C	T_{NI} / °C	ΔH_{Cr-} / kJmol^{-1}	$\Delta H_{N_{TB}N}$/ kJmol^{-1}	ΔH_{NI} / kJmol^{-1}	ΔS_{Cr-} /R	$\Delta S_{N_{TB}N}$ /R	ΔS_{NI} /R
108	73	151	35.98	0.01	1.16	22.73	0.004	0.33

Table 3. The transitional properties of CBO5O.4.

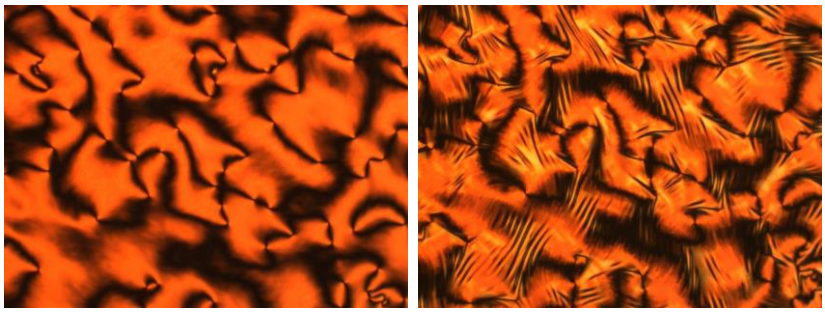

Figure 7. The nematic schlieren (left) and twist-bend nematic (right) textures shown by CBO5O.4 in a 1.6 µm with homeotropic anchoring.

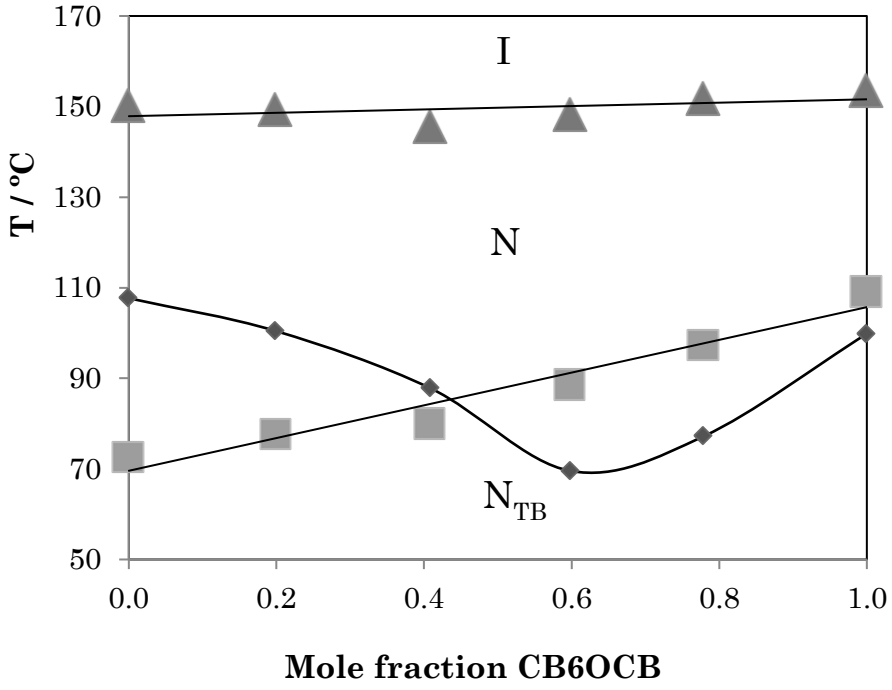

Figure 8. Phase diagram constructed for binary mixtures of CBO5O.4 and CB6OCB. Triangles represent nematic-isotropic transition temperatures, squares twist-bend nematic-nematic transition temperatures, and diamonds the melting points.

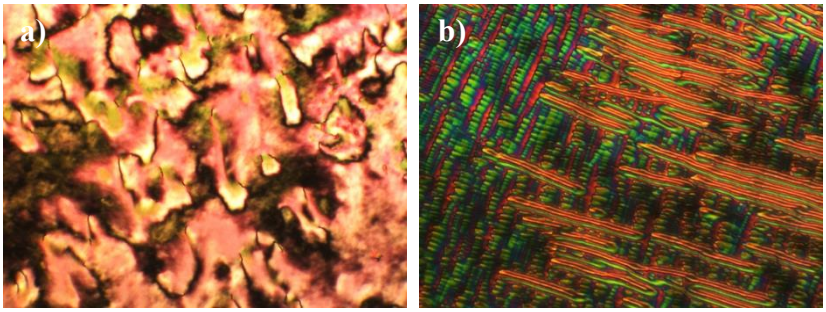

Figure 9. (a) The schlieren nematic texture and (b) the polygonal and rope-like textures characteristic of the N_{TB} phase of a CBO5O.4 / CB6OCB mixture containing 80 mol % CBO5O.4

Figure 10 compares T_{NI} and $T_{N_{TB}N}$ for the CB6O.*m* and CB6O.O*m* series, and for both transitions the CB6O.O*m* series shows the higher values. The increase

in T_{NI} on passing from a methylene-linked to an ether-linked terminal alkyl chain may be attributed to the change in the average shape of the molecule and specifically the angle the chain makes with the phenyl ring to which it is attached, see Figure 11. Thus, an alkyloxy chain lies more or less in plane with the ring to which it is attached whereas an alkyl chain protrudes at some angle. The greater shape anisotropy of the former accounts for the higher values of T_{NI} observed. Presumably a similar argument holds for the higher values of $T_{N_{TB}N}$ seen for the CB6O.O*m* series and the more uniform molecular curvature arising from the alkyloxy chain assists the packing of these bent molecules.

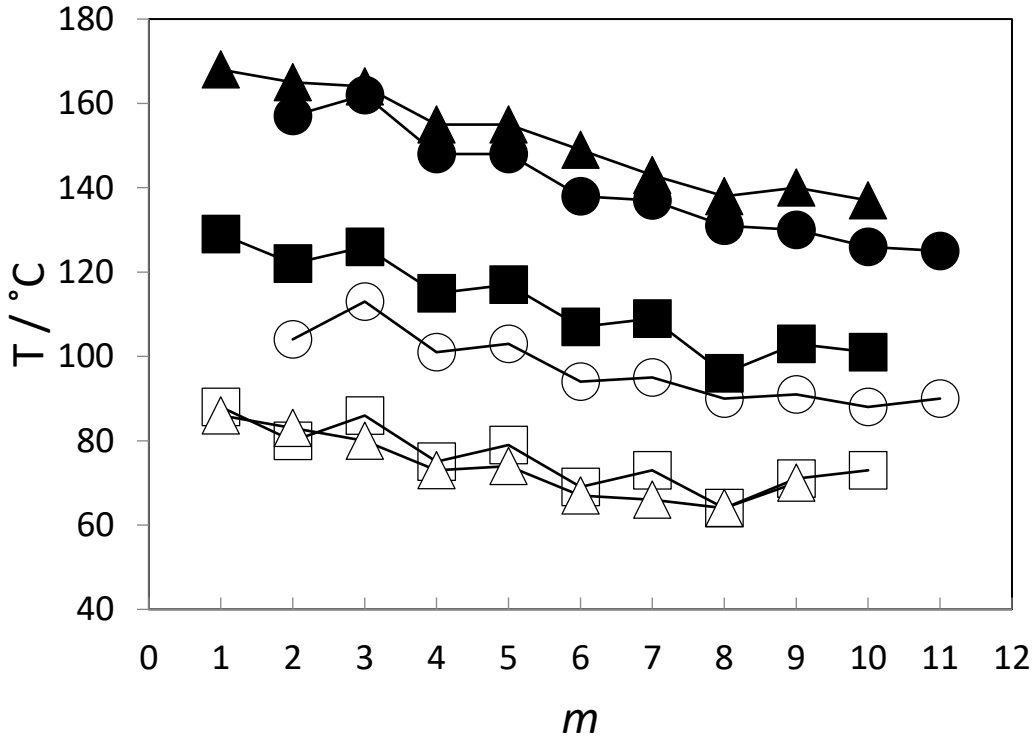

Figure 10. The dependence of the nematic-isotropic transition temperature, T_{NI}, (filled symbols) and the twist-bend nematic-isotropic transition temperature, $T_{N_{TB}N}$, (open symbols) on the number of carbon atoms in the terminal alkyl chain, *m*, for the CBO5O.*m* (triangles), and CB6O.*m* (squares) series. Also shown are the corresponding transition temperatures for the CB6O.O*m* series (circles) for which *m*+1 has been plotted in order to compare compounds having terminal chains having the same parity.

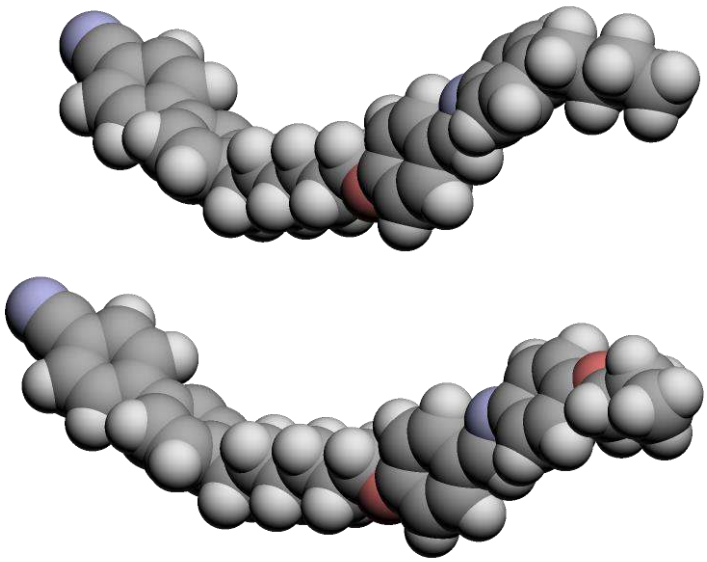

Figure 11. The shapes of CB6O.4 (top) and CB6O.O3 (bottom) with the spacers in the all-*trans* conformation showing the difference in the disposition of the terminal chain with respect to the group to which it is attached.

Figure 10 also shows the nematic-isotropic transition temperatures for the CBO5O.*m* series, and these are marginally higher than those of the CB6O.O*m* series, but significantly higher than those of the corresponding CB6O.*m* series. The difference between the values of T_{NI} for corresponding members of the CBO5O.*m* and CB6O.*m* series are in complete accord with predictions of a theoretical model developed by Luckhurst and co-workers [60-62] in which the only difference between the dimers is their shape and specifically, the bond angle between the *para* axis of the mesogenic unit and the first bond in the spacer. This angle is larger for the ether link and hence, the ether-linked dimer is more linear, see Figure 12. This greater shape anisotropy accounts for the higher T_{NI} observed. This view was supported by calculated T_{NI} values using a molecular field theory in which the only difference in the calculations for the two series was this bond angle [60]. This approach also predicts that $\Delta S_{NI}/R$ for the ether-linked materials are higher than those of the corresponding methylene-linked dimers and this is consistent with the data shown in Figure 13. The similar values of T_{NI} seen for the CBO5O.*m* and CB6O.O*m* series suggest that the

change in shape due to replacing an ether- by a methylene-link between the spacer and mesogenic group is almost offset by replacing a methylene- by an ether-link between the terminal chain and mesogenic group. It is apparent, however, that the values of $\Delta S_{NI}/R$ are similar for the CB6O.*m* and CB6O.O*m* series, whereas those for the CBO5O.O*m* series are significantly higher, see Figure 13, in accord with the theoretical predictions referred to earlier [61].

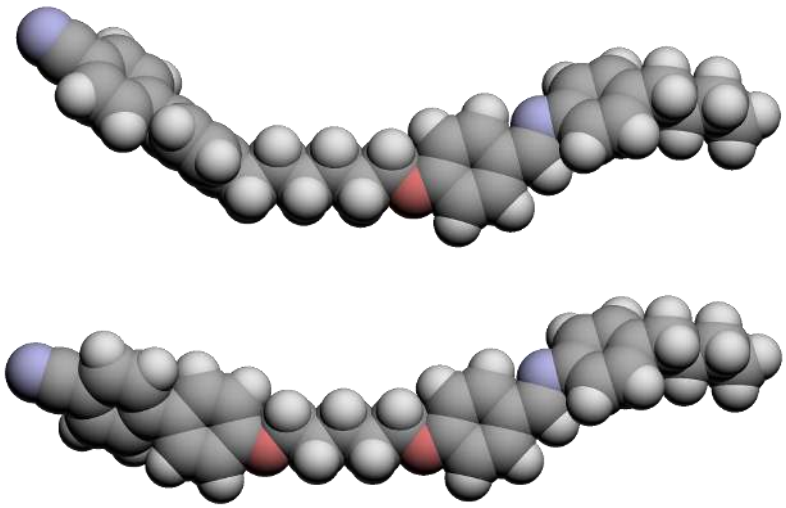

Figure 12. The shapes of CB6O.4 (top) and CBO5O.4 (bottom) with the spacers in the all-*trans* conformation showing the more linear structure of the latter.

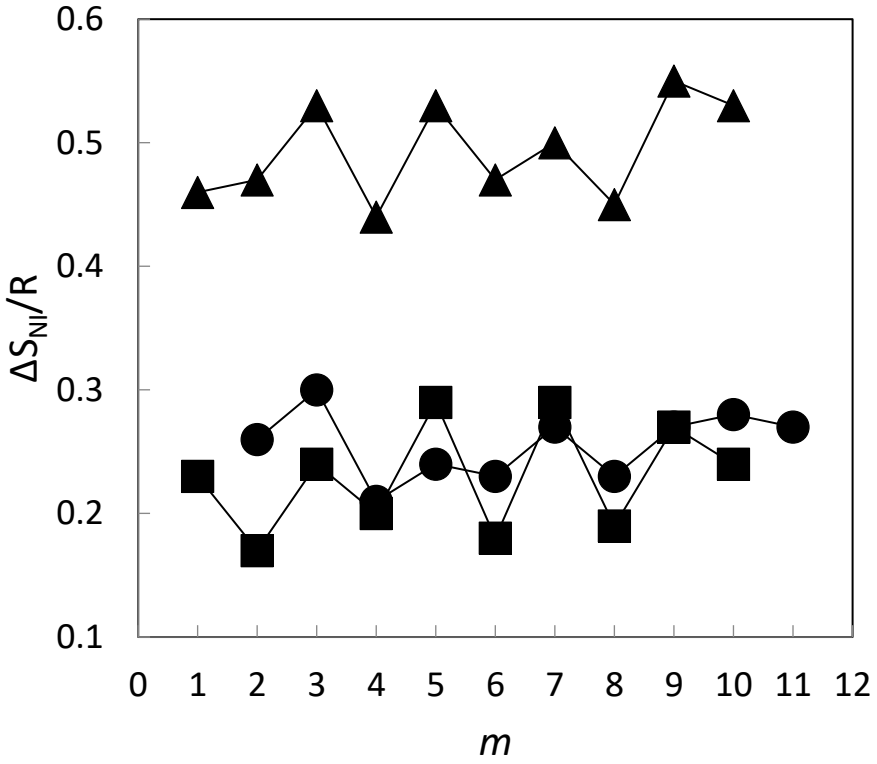

Figure 13. The dependence of the entropy change associated with the nematic-isotropic transition, $\Delta S_{NI}/R$, on the number of carbon atoms in the terminal alkyl chain, *m*, for the CBO5O.*m* (triangles), and CB6O.*m* (squares) series. Also shown are the corresponding $\Delta S_{NI}/R$ values for the CB6O.O*m* series (circles) for which *m*+1 has been plotted in order to compare compounds having terminal chains having the same parity.

If we now consider the values of $T_{N_{TB}N}$ shown by these three series, see Figure 10, it is quite clear that the CB6O.O*m* series shows the highest values. Surprisingly, the values of $T_{N_{TB}N}$ shown by corresponding members of the CB6O.*m* and CBO5O.*m* series are very similar. This is an unexpected observation given that for other series of dimers changing the spacer from $-(CH_2)_6O-$ to $-O(CH_2)_5O-$ leads to a significant decrease in $T_{N_{TB}N}$ and this has been attributed to the more bent shape shown by the $-(CH_2)_6O-$ linked dimers[19, 26, 53], see Figure 12. We have seen in Figure 10 that the CBO5O.*m* series shows considerably higher values of T_{NI} than the corresponding members of the CB6O.*m* series and that this may be understood in

terms of the difference in shape between the two series arsing from the nature of the links between the spacer and the mesogenic units, see Figure 12. Specifically, the CBO5O.*m* dimers are more linear than their CB6O.*m* counterparts. Paradoxically, however, the similarity in the values of $T_{N_{TB}N}$ exhibited by these two series could be interpreted as indicating that the CBO5O.*m* and CB6O.*m* series are *similar* in shape. It is certainly noteworthy that for the pair of dimers studied in detail here, the more linear CBO5O.4 shows a higher value of $T_{N_{TB}N}$ than CB6O.4. This indicates that shape alone cannot account for the behaviour of these dimers.

Instead, the behaviour of this class of non-symmetric dimers is thought, at least in part, to be driven by a specific interaction between the unlike mesogenic units [46, 48, 49]. The exact nature of this interaction is unclear but has been suggested to be an electrostatic quadrupolar interaction between groups having quadrupoles of opposite signs [63]. The importance of the mixed mesogenic unit interaction in determining the phase behaviour of nonsymmetric dimers may be assessed by comparing their nematic-isotropic transition temperatures to the average of those of the parent symmetric dimers. This comparison is normally expressed in terms of a scaled deviation, ΔT_{SC}, given by [49]:

$$\Delta T_{SC} = \frac{2T_{AB} - (T_A + T_B)}{T_A + T_B}$$

where T_{AB} is the T_{NI} of the non-symmetric dimer, and T_A and T_B those of the corresponding symmetric dimers, CBO5OCB, CB7CB [53] and the *m*.O5O.*m* series [64]. Figure 14 shows the dependence of ΔT_{SC} on *m* for the CB6O.*m* and CBO5O.*m* series and the values for the CBO5O.*m* series are, albeit marginally, higher. Within the framework of a molecular field theory developed to predict phase diagrams for binary mixtures of nematogens A and B, three intermolecular energy parameters are required: ε_{AA}, ε_{BB} and the mixed parameter, ε_{AB} [65]. If ε_{AB} is assumed to be the geometric mean of ε_{AA} and ε_{BB} then T_{NI} for the mixture is simply the weighted average of those of the two components and $\Delta T_{SC} = 0$. A positive deviation in ε_{AB} from the geometric mean approximation gives $\Delta T_{SC} > 0$ whereas a negative deviation yields $\Delta T_{SC} < 0$. Even small values of ε_{AB} from the geometric mean approximation such as ±1.85% give curved T_{NI} lines in the predicted phase diagram [65, 66]. The relatively small values of ΔT_{SC} exhibited by the non-symmetric dimers suggest that

the deviation in ε_{AB} from the geometric mean approximation is also small but significant. Thus, the higher values of ΔT_{SC} seen for the CBO5O.*m* series indicate that an enhanced specific interaction exists between the unlike mesogenic units in this series suggesting that this may be at the root of the higher than expected $T_{N_{TB}N}$ values, by providing an additional driving force for the local packing of these bent molecules.

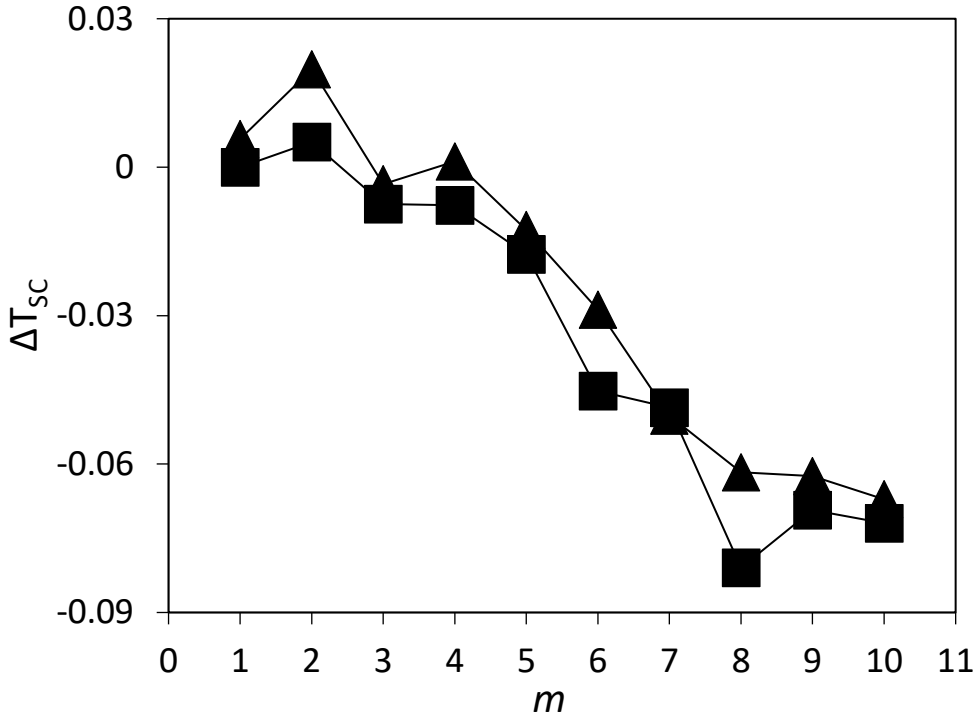

Figure 14. The dependence of ΔTSC on the number of carbon atoms in the terminal alkyl chain, *m*, for the CBO5O.*m* (triangles), and CB6O.*m* (squares) series.

Conclusions

It is widely-accepted that the predominant structural feature driving the formation of the N_{TB} phase appears to be molecular curvature and this is consistent with predictions made using a generalised Maier-Saupe theory for which $T_{N_{TB}N}$ is shown to be highly sensitive to the bend angle [12]. The surprising similarity between the $T_{N_{TB}N}$ values for corresponding members of the CBO5O.*m* and CB6O.*m* series, however, reinforces the view that shape alone cannot account for the differences in

$T_{N_{TB}N}$ between systems having similar molecular structures. Instead the more favourable specific interactions between the unlike mesogenic units in the CBO5O.*m* series may serve to promote the formation of the N_{TB} phase.

The majority of N_{TB} phases reported to date show locally intercalated packing of the molecules and it has been suggested that this provides an important driving force in the formation of the phase. Increasing the terminal chain length in the CB6O.*m* series changes the local structure found in the N and N_{TB} phases from being intercalated, through interdigitated to bilayer but with no apparent impact on the stability of the phases. This suggests that the importance of the intercalation of the molecules may have been overstated.

Smectic behaviour is only observed in the CB6O.*m* and CBO5O.*m* series for the decyl members, and this notable absence of smectic behaviour may be attributed to the difficulty of packing these bent molecules into a layered structure which is further exacerbated by the terminal alkyl chain that protrudes at an angle from the Schiff base moiety. By comparison, smectic behaviour is observed for intermediate chain lengths of the CB6O.O*m* series in which the terminal alkoxy chain now lies in the plane of the phenyl ring to which it is attached presumably allowing for a more efficient packing of the molecules into layers [44].

Acknowledgements

EG and DP acknowledge the support of the National Science Centre (Poland): (Grant Number 2016/22/A/ST5/00319). RW gratefully acknowledges The Carnegie Trust for the Universities of Scotland for funding the award of a PhD scholarship.

References

1. M. Cestari, S. Diez-Berart, D. A. Dunmur, A. Ferrarini, M. R. de la Fuente, D. J. B. Jackson, D. O. Lopez, G. R. Luckhurst, M. A. Perez-Jubindo, R. M. Richardson, J. Salud, B. A. Timimi and H. Zimmermann, *Phys. Rev. E*, 2011, **84**, 031704.
2. V. Borshch, Y. K. Kim, J. Xiang, M. Gao, A. Jakli, V. P. Panov, J. K. Vij, C. T. Imrie, M. G. Tamba, G. H. Mehl and O. D. Lavrentovich, *Nature Commun.*, 2013, **4**, 2635.

3. C. H. Zhu, M. R. Tuchband, A. Young, M. Shuai, A. Scarbrough, D. M. Walba, J. E. Maclennan, C. Wang, A. Hexemer and N. A. Clark, *Phys Rev Lett*, 2016, **116**, 147803.
4. R. B. Meyer, in *Structural problems in liquid crystal physics, Les houches summer school in theoretical physics*, eds. R. Balian and W. G, Gordon and Breach, New York, 1976, pp. 273-373.
5. I. Dozov, *Europhys. Lett.*, 2001, **56**, 247-253.
6. A. A. Dawood, M. C. Grossel, G. R. Luckhurst, R. M. Richardson, B. A. Timimi, N. J. Wells and Y. Z. Yousif, *Liq. Cryst.*, 2016, **43**, 2-12.
7. A. A. Dawood, M. C. Grossel, G. R. Luckhurst, R. M. Richardson, B. A. Timimi, N. J. Wells and Y. Z. Yousif, *Liq. Cryst.*, 2017, **44**, 106-126.
8. C. T. Archbold, E. J. Davis, R. J. Mandle, S. J. Cowling and J. W. Goodby, *Soft Matter*, 2015, **11**, 7547-7557.
9. J. Xiang, Y. N. Li, Q. Li, D. A. Paterson, J. M. D. Storey, C. T. Imrie and O. D. Lavrentovich, *Adv. Mater.*, 2015, **27**, 3014-3018.
10. J. Xiang, A. Varanytsia, F. Minkowski, D. A. Paterson, J. M. D. Storey, C. T. Imrie, O. D. Lavrentovich and P. Palffy-Muhoray, *Proc. Natl Acad. Sci. USA*, 2016, **113**, 12925-12928.
11. S. M. Salili, J. Xiang, H. Wang, Q. Li, D. A. Paterson, J. M. D. Storey, C. T. Imrie, O. D. Lavrentovich, S. N. Sprunt, J. T. Gleeson and A. Jakli, *Phys. Rev. E*, 2016, **94**, 042705.
12. C. Greco, G. R. Luckhurst and A. Ferrarini, *Soft Matter*, 2014, **10**, 9318-9323.
13. C. T. Imrie and P. A. Henderson, *Chem. Soc. Rev.*, 2007, **36**, 2096-2124.
14. C. T. Imrie, P. A. Henderson and G.-Y. Yeap, *Liq. Cryst.*, 2009, **36**, 755-777.
15. M. Sepelj, A. Lesac, U. Baumeister, S. Diele, H. L. Nguyen and D. W. Bruce, *J. Mater. Chem.*, 2007, **17**, 1154-1165.
16. V. P. Panov, M. Nagaraj, J. K. Vij, Y. P. Panarin, A. Kohlmeier, M. G. Tamba, R. A. Lewis and G. H. Mehl, *Phys. Rev. Lett.*, 2010, **105**, 167801.
17. P. A. Henderson and C. T. Imrie, *Liq. Cryst.*, 2011, **38**, 1407-1414.
18. N. Sebastian, D. O. Lopez, B. Robles-Hernandez, M. R. de la Fuente, J. Salud, M. A. Perez-Jubindo, D. A. Dunmur, G. R. Luckhurst and D. J. B. Jackson, *Phys. Chem. Chem. Phys.*, 2014, **16**, 21391-21406.
19. Z. B. Lu, P. A. Henderson, B. J. A. Paterson and C. T. Imrie, *Liq. Cryst.*, 2014, **41**, 471-483.
20. R. J. Mandle, C. C. A. Voll, D. J. Lewis and J. W. Goodby, *Liq. Cryst.*, 2016, **43**, 13-21.
21. R. J. Mandle and J. W. Goodby, *Chem. Eur. J.*, 2016, **22**, 9366-9374.
22. C. T. Archbold, J. L. Andrews, R. J. Mandle, S. J. Cowling and J. W. Goodby, *Liq. Cryst.*, 2017, **44**, 84-92.
23. V. P. Panov, J. K. Vij and G. H. Mehl, *Liq. Cryst.*, 2017, **44**, 147-159.
24. A. Lesac, U. Baumeister, I. Dokli, Z. Hamersak, T. Ivsic, D. Kontrec, M. Viskic, A. Knezevic and R. J. Mandle, *Liq. Cryst.*, 2018, **45**, 1101-1110.
25. C. T. Archbold, R. J. Mandle, J. L. Andrews, S. J. Cowling and J. W. Goodby, *Liq. Cryst.*, 2017, **44**, 2079-2088.
26. D. A. Paterson, R. Walker, J. P. Abberley, J. Forestier, W. T. A. Harrison, J. M. D. Storey, D. Pociecha, E. Gorecka and C. T. Imrie, *Liq. Cryst.*, 2017, **44**, 2060-2078.

27. D. A. Paterson, J. Xiang, G. Singh, R. Walker, D. M. Agra-Kooijman, A. Martinez-Felipe, M. Gan, J. M. D. Storey, S. Kumar, O. D. Lavrentovich and C. T. Imrie, *J. Am. Chem. Soc.*, 2016, **138**, 5283-5289.
28. K. Watanabe, T. Tamura, S. M. Kang and M. Tokita, *Liq. Cryst.*, 2018, **45**, 924-930.
29. J. P. Abberley, S. M. Jansze, R. Walker, D. A. Paterson, P. A. Henderson, A. T. M. Marcelis, J. M. D. Storey and C. T. Imrie, *Liq Cryst*, 2017, **44**, 68-83.
30. W. D. Stevenson, H. X. Zou, X. B. Zeng, C. Welch, G. Ungar and G. H. Mehl, *Phys Chem Chem Phys*, 2018, **20**, 25268-25274.
31. D. Chen, M. Nakata, R. F. Shao, M. R. Tuchband, M. Shuai, U. Baumeister, W. Weissflog, D. M. Walba, M. A. Glaser, J. E. Maclennan and N. A. Clark, *Phys. Rev. E*, 2014, **89**, 022506.
32. S. P. Sreenilayam, V. P. Panov, J. K. Vij and G. Shanker, *Liq. Cryst.*, 2017, **44**, 244-253.
33. R. J. Mandle and J. W. Goodby, *RSC Adv.*, 2016, **6**, 34885-34893.
34. R. J. Mandle, M. P. Stevens and J. W. Goodby, *Liq. Cryst.*, 2017, **44**, 2046-2059.
35. R. J. Mandle and J. W. Goodby, *Angew Chem Int Ed*, 2018, **57**, 7096-7100.
36. S. M. Jansze, A. Martinez-Felipe, J. M. D. Storey, A. T. M. Marcelis and C. T. Imrie, *Angew. Chem. Int. Ed.*, 2015, **54**, 643-646.
37. D. A. Paterson, A. Martinez-Felipe, S. M. Jansze, A. T. M. Marcelis, J. M. D. Storey and C. T. Imrie, *Liq. Cryst.*, 2015, **42**, 928-939.
38. R. Walker, D. Pociecha, J. P. Abberley, A. Martinez-Felipe, D. A. Paterson, E. Forsyth, G. B. Lawrence, P. A. Henderson, J. M. D. Storey, E. Gorecka and C. T. Imrie, *Chem. Commun.*, 2018, **54**, 3383-3386.
39. R. J. Mandle and J. W. Goodby, *Crystengcomm*, 2016, **18**, 8794-8802.
40. R. J. Mandle and J. W. Goodby, *Soft Matter*, 2016, **12**, 1436-1443.
41. N. Sebastian, M. G. Tamba, R. Stannarius, M. R. de la Fuente, M. Salamonczyk, G. Cukrov, J. Gleeson, S. Sprunt, A. Jakli, C. Welch, Z. Ahmed, G. H. Mehl and A. Eremin, *Phys. Chem. Chem. Phys.*, 2016, **18**, 19299-19308.
42. J. P. Abberley, R. Killah, R. Walker, J. M. D. Storey, C. T. Imrie, M. Salamonczyk, C. H. Zhu, E. Gorecka and D. Pociecha, *Nature Commun.*, 2018, **9**, 228.
43. S. P. Sreenilayam, Y. P. Panarin, J. K. Vij, V. P. Panov, A. Lehmann, M. Poppe, M. Prehm and C. Tschierske, *Nature Commun.*, 2016, **7**, 11369.
44. D. A. Paterson, C. A. Crawford, D. Pociecha, R. Walker, J. M. D. Storey, E. Gorecka and C. T. Imrie, *Liq Cryst*, 2018, **45**, 2341-2351.
45. D. Pociecha, C. A. Crawford, D. A. Paterson, J. M. D. Storey, C. T. Imrie, N. Vaupotic and E. Gorecka, *Phys. Rev. E*, 2018, **98**, 052706.
46. C. T. Imrie, *Liq. Cryst.*, 2006, **33**, 1449-1454.
47. D. A. Paterson, M. Gao, Y. K. Kim, A. Jamali, K. L. Finley, B. Robles-Hernandez, S. Diez-Berart, J. Salud, M. R. de la Fuente, B. A. Timimi, H. Zimmermann, C. Greco, A. Ferrarini, J. M. D. Storey, D. O. Lopez, O. D. Lavrentovich, G. R. Luckhurst and C. T. Imrie, *Soft Matter*, 2016, **12**, 6827-6840.
48. J. L. Hogan, C. T. Imrie and G. R. Luckhurst, *Liq. Cryst.*, 1988, **3**, 645-650.
49. G. S. Attard, R. W. Date, C. T. Imrie, G. R. Luckhurst, S. J. Roskilly, J. M. Seddon and L. Taylor, *Liq. Cryst.*, 1994, **16**, 529-581.

50. C. T. Imrie, P. A. Henderson and J. M. Seddon, *J. Mater. Chem.*, 2004, **14**, 2486-2488.
51. R. J. Mandle, E. J. Davis, C. C. A. Voll, C. T. Archbold, J. W. Goodby and S. J. Cowling, *Liq. Cryst.*, 2015, **42**, 688-703.
52. T. Ivsic, M. Vinkovic, U. Baumeister, A. Mikleusevic and A. Lesac, *RSC Advances*, 2016, **6**, 5000-5007.
53. D. A. Paterson, J. P. Abberley, W. T. Harrison, J. M. D. Storey and C. T. Imrie, *Liq. Cryst.*, 2017, **44**, 127-146.
54. J. W. Emsley, G. De Luca, A. Lesage, D. Merlet and G. Pileio, *Liq. Cryst.*, 2007, **34**, 1071-1093.
55. M. Tarini, P. Cignoni and C. Montani, *IEEE Trans. Visualization and Computer Graphics*, 2006, **12**, 1237-1244.
56. P. A. Henderson, O. Niemeyer and C. T. Imrie, *Liq. Cryst.*, 2001, **28**, 463-472.
57. P. A. Henderson, J. M. Seddon and C. T. Imrie, *Liq. Cryst.*, 2005, **32**, 1499-1513.
58. M. Salamonczyk, N. Vaupotic, D. Pociecha, R. Walker, J. M. D. Storey, C. T. Imrie, C. Wang, C. Zhu and E. Gorecka, *Submitted*, 2018.
59. C. T. Imrie and L. Taylor, *Liq. Cryst.*, 1989, **6**, 1-10.
60. A. P. J. Emerson and G. R. Luckhurst, *Liq. Cryst.*, 1991, **10**, 861-868.
61. A. Ferrarini, G. R. Luckhurst, P. L. Nordio and S. J. Roskilly, *J. Chem. Phys.*, 1994, **100**, 1460-1469.
62. A. Ferrarini, G. R. Luckhurst, P. L. Nordio and S. J. Roskilly, *Liq. Cryst.*, 1996, **21**, 373-382.
63. A. E. Blatch, I. D. Fletcher and G. R. Luckhurst, *Liq. Cryst.*, 1995, **18**, 801-809.
64. R. W. Date, C. T. Imrie, G. R. Luckhurst and J. M. Seddon, *Liq. Cryst.*, 1992, **12**, 203-238.
65. R. Humphries, P. James and G. R. Luckhurst, *Symp. Faraday Soc.*, 1971, **5**, 107-118.
66. R. L. Humphries and G. R. Luckhurst, *Chem. Phys. Lett.*, 1973, **23**, 567-570.